Extremes, intermittency, and time directionality of atmospheric turbulence at the crossover from production to inertial scales

E. Zorzetto*
Division of Earth and Ocean Sciences, Nicholas School of the Environment, Duke University, Durham, North Carolina 27708, USA

A. D. Bragg†
Department of Civil and Environmental Engineering, Duke University, Durham, North Carolina 27708, USA

G. Katul‡
Nicholas School of the Environment, Duke University, Durham, North Carolina 27708, USA and IMK-IFU, The Karlsruher Institut für Technologie, Kreuzeckbahnstraße 19, 82467 Garmisch-Partenkirchen, Germany

(Received 4 December 2017; published 10 September 2018)

The effects of mechanical generation of turbulent kinetic energy and buoyancy forces on the statistics of air temperature and velocity increments are experimentally investigated at the crossover from production to inertial range scales. The ratio of an approximated mechanical to buoyant production (or destruction) of turbulent kinetic energy can be used to form a dimensionless stability parameter ζ that classifies the state of the atmosphere as common in many atmospheric surface layer studies. We assess how ζ affects the scalewise evolution of the probability of extreme air temperature excursions, their asymmetry, and time directionality. The analysis makes use of high-frequency turbulent velocity and air temperature time-series measurements collected at $z = 5$ m above a grass surface at very large frictional Reynolds numbers $\mathrm{Re}_* = u_* z/\nu > 1 \times 10^5$ (u_* is the friction velocity and ν is the kinematic viscosity of air). A multitime measure of the imbalance between forward and backward phase-space trajectories is employed to investigate the time-directional properties of the scalar (temperature) field. Using conventional higher-order structure functions, we find that temperature exhibits larger intermittency and wider multifractality when compared to the longitudinal velocity component, consistent with laboratory studies and simulations conducted at lower Re_*. We find that the magnitude of ζ, rather than the sign of the heat flux, impacts the distribution of scalar increments at separation scales well within the inertial subrange. Conversely, the direction of the heat flux fingerprints the observed time-directionality properties of the scalar field in the first two decades of inertial subrange scales. These combined findings demonstrate that external boundary conditions, and in particular the magnitude and sign of the sensible heat flux, have a significant impact on temperature advection-diffusion dynamics within the inertial range.

DOI: 10.1103/PhysRevFluids.3.094604

*enrico.zorzetto@duke.edu
†andrew.bragg@duke.edu
‡gaby@duke.edu

I. INTRODUCTION

Turbulence in fluids is prototypical of spatially extended nonlinear dissipative systems characterized by large fluctuations that are active over wide-ranging scales [1]. The dynamics of a substance or scalar advected by a turbulent flow (often termed scalar turbulence [2]) is by no means an exception to this description. Scalar turbulence shares many phenomenological parallels with the much studied turbulent velocity fluctuations, especially in the inertial subrange. However, scalar turbulence also exhibits distinctive large- and fine-scaled temporal patterns (e.g., ramp-cliff patterns) that are usually weak or altogether absent from their componentwise turbulent velocity counterparts [2–4]. This finding is particularly true in the atmospheric surface layer (ASL) [5,6], a layer within the atmospheric boundary layer that is sufficiently far above roughness elements but not too far from the ground to be directly impacted by the Coriolis force. In the ASL, the frictional Reynolds number $\mathrm{Re}_* = u_* z/\nu$ can readily exceed 10^5, where z is the distance above the ground surface, u_* is the friction velocity related to the kinematic turbulent stress, and ν is the kinematic viscosity of air. A direct consequence of this large Re_* is a wide separation between scales over which turbulent kinetic energy k is produced and dissipated. In the absence of thermal stratification, k is produced at scales commensurate with z; however, the action of fluid viscosity responsible for the dissipation of k occurs at scales commensurate with or smaller than the Kolmogorov microscale $\eta_K = (\nu^3/\langle\epsilon\rangle)^{1/4}$, where $\langle\epsilon\rangle$ is the mean turbulent kinetic energy dissipation rate that is proportional to u_*^3/z for a neutrally stratified ASL [6]. These estimates of $\langle\epsilon\rangle$ and η_K result in $z/\eta_K \sim \mathrm{Re}_*^{3/4} > 5000$ in the ASL, which is rarely achieved in direct numerical simulations or laboratory studies. Embedded in this wide-ranging scale separation is the inertial subrange [7], where self-similar scaling of velocity and air temperature structure functions is expected to hold for eddy sizes much larger than η_K but much smaller than z. Integral scales or scales comparable to z are directly influenced by boundary conditions imposed on the flow including surface heating (or cooling) in the ASL, whereas small scales (e.g., η_K) may attain universality and local isotropy after a large number of cascading steps away from the energy injection scales.

Much attention has been historically dedicated to the inertial subrange and the subsequent crossover to the viscous or molecular regimes precisely because of the possible universal character of turbulence at such fine scales [4,8–12]. However, it is now accepted that some coupling between small and large scales exists, especially for passive scalars [2,4,13], that act to enhance intermittency buildup across scales and distort any universal behavior by injecting the effects of the boundary conditions (or the k generation mechanism). Along similar lines of inquiry, it has been conjectured that the presence of coherent ramp-cliff patterns in concentration (or temperature) time series are responsible, to some degree, for this coupling [4]. Ramp-cliff structures are characterized by local intense scalar gradients separated by large quiescent regions. The presence of ramp-cliff structures in scalar time series has been shown to break locality of eddy interactions and determine some departures from small-scale isotropy.

Sweep-ejection dynamics connected to the presence of ramps are likely to play a major role in observed extreme value statistics, as shown, e.g., for Lagrangian velocity sequences in plant canopy turbulence [14]. Moreover, ramps are asymmetric and produce nonzero odd-ordered structure functions, sharing a striking resemblance to flight-crash events recently reported for the turbulent kinetic energy of Lagrangian particles [15]. Even though ramps have been extensively observed experimentally [3], studied as surface renewal processes [13], and from a Lagrangian perspective [2,16], a unified picture describing their effects on inertial scales statistics remains lacking and motivates the work here.

Our main objective is to investigate two questions about scalar turbulence at scales spanning production to inertial subranges: how ramp-cliff patterns modify (i) the probability of extreme scalar concentration or air temperature excursions and its corollary intermittency buildup and (ii) symmetry and time reversibility of scalar turbulence. These two questions are explored for differing turbulent energy injection mechanisms (mechanical and buoyancy forces) in the ASL. Here we focus on the production-to-inertial scales instead of the usual inertial to viscous ranges for the

following reasons. First, any cross-scale coupling with ramp-cliff patterns is likely to be sensed at large scales commensurate with the ramp durations. Second, these scales are deemed most relevant when constructing subgrid-scale models for improving large-eddy simulations [17–20]. Third, these scales encode much of the scalar variance that is needed when deriving phenomenological theories for the bulk flow properties based on the spectral shapes of the turbulent velocity and air temperature [21–25], especially for the ASL.

To achieve the study objectives, high-frequency measurements of the three velocity components and air temperature fluctuations in the ASL are used to explore flow statistics at the transition from production to inertial scales. In particular, the focus is on the first two decades dominated by approximate inertial subrange effects, where the transition from the large eddies to the universal equilibrium or inertial range occurs. The statistical properties of temperature increments within this range of scales are examined with the goal of addressing to what extent the tail properties (and thus the probability of extreme events) at fine scales still carry signatures from the production ranges and in particular of large coherent structures such as ramp-cliff structures. The experiments here span several atmospheric stability regimes that dictate to what degree turbulent kinetic energy is mechanically or buoyantly generated (or dissipated) depending on surface heating (or cooling) and on the turbulent shear stress near the ground [26]. However, due to the large Reynolds number encountered in the ASL, the stable stratification is not sufficiently severe to allow for a transition to nonturbulent regimes. Therefore, the turbulence can be studied as three dimensional and fully developed.

The paper is organized as follows. In Sec. II the budget for turbulent kinetic energy forced by a mean velocity gradient and buoyancy is reviewed so as to define the key variables and dimensionless quantities pertinent to ASL flows. Then the statistical tools used to characterize intermittency and time directionality of the scalar field are introduced. Section III presents the experimental setup and data processing and compares the outcome of this experiment with predictions from traditional turbulence theory in the inertial subrange. The results obtained investigating extreme values and time-directional properties for velocity and temperature are then presented in Sec. IV. In Sec. V the main conclusions are featured. The Appendix shows that distortions of the inertial range due to stable stratification are not relevant for the range of scales studied here.

II. THEORY

A. Overview of ASL similarity at large and small scales

The turbulent kinetic energy budget for a stationary and planar homogeneous flow in the absence of subsidence is given by

$$\frac{\partial k}{\partial t_0} = 0 = -\overline{u'w'}\frac{dU}{dz} + \beta_0 g\overline{w'T'} + P_D + T_T - \epsilon, \tag{1}$$

where $k = (\overline{u'^2 + v'^2 + w'^2})/2$ is the turbulent kinetic energy; u', v', and w' are the turbulent velocity components along the mean wind (x), lateral (y), and vertical (z) directions, respectively; t_0 is time; the five terms on the right-hand side are mechanical production, buoyant production (or destruction), pressure transport, turbulent transport of k, and viscous dissipation of k, respectively; β_0 is the thermal expansion coefficient for gases ($\beta_0 = 1/T$, with T the air temperature here); g is the gravitational acceleration; $-\overline{u'w'} = u_*^2$ is the turbulent kinematic shear stress near the surface; and $\overline{w'T'}$ is the kinematic sensible heat flux from (or to) the surface. When $\overline{w'T'} > 0$, buoyancy is responsible for the generation of k and the ASL is classified as unstable. When $\overline{w'T'} < 0$, the ASL is classified as stable and buoyancy acts to diminish the mechanical production of k. The relative significance of the mechanical production with respect to the buoyancy generation (or destruction)

may be expressed as

$$-\overline{u'w'}\frac{dU}{dz} + \beta_0 g\overline{w'T'} = \frac{u_*^3}{\kappa z}\left[\phi_m(\zeta) + \frac{\kappa z\beta_0 g\overline{w'T'}}{u_*^3}\right] = \frac{u_*^3}{\kappa z}[\phi_m(\zeta) - \zeta], \tag{2}$$

where

$$\frac{dU}{dz} = \frac{u_*}{\kappa z}\phi_m(\zeta), \quad \zeta = \frac{z}{L}, \quad L = -\frac{u_*^3}{\kappa g\beta_0\overline{w'T'}}, \tag{3}$$

$\phi_m(\zeta)$ is known as a stability correction function reflecting the effects of thermal stratification on the mean velocity gradient [$\phi_m(0) = 1$ recovers the von Kármán-Prandtl logarithmic law], $\kappa \approx 0.4$ is the von Kármán constant, and L is known as the Obukhov length as described by the Monin-Obukhov similarity theory [26]. The physical interpretation of L is that it is the height at which mechanical production balances the buoyant production or destruction when $\phi_m(\zeta)$ does not deviate appreciably from unity. For a neutrally stratified ASL flow, $|L| \to \infty$ and $|\zeta| \to 0$. The sign of L reflects the direction of the heat flux, with negative values of L corresponding to upward heat fluxes (unstable atmospheric conditions) and positive values of L corresponding to downward heat flux (stable atmosphere).

Several bulk flow statistics in the ASL can be reasonably described by the aforementioned Monin-Obukhov similarity theory, including the mean air temperature gradient dT/dz and the air temperature variance $\overline{T'^2}$, both varying with ζ when normalized by a temperature scale $T_* = -\overline{w'T'}/u_*$. However, the statistics of some large-scale features within the temperature time-series traces, such as the statistics of ramp-cliff patterns, do not scale with z. For starters, the ramp characteristic dimension is generally larger than z and its duration exceeds the mean vorticity timescale $[\kappa z\phi_m(\zeta)^{-1}]u_*^{-1}$. Ramps have been observed within canopies, near the canopy atmosphere interface, and other types of flows as reviewed elsewhere [4,13]. While z/L may not be the proper scaling parameter for ramps, it does indirectly impact many of their features in air temperature time traces sampled within the ASL. For example, in stably stratified ASL flows, the temperature ramps appear inverted when compared to their near-neutral counterparts. The amplitudes and durations of ramps can increase with increasing instability due to weaker shearing and intense buoyant updrafts [27,28].

At small scales associated with the inertial subrange, the velocity and temperature second-order structure functions are commonly described by the Kolmogorov theory [7] given as

$$S_u^2(r) = \overline{[\Delta u(r)]^2} = 4C_{0,u}(\langle\epsilon\rangle r)^{2/3}, \tag{4}$$

$$S_w^2(r) = \overline{[\Delta w(r)]^2} = 4C_{0,w}(\langle\epsilon\rangle r)^{2/3}, \tag{5}$$

$$S_T^2(r) = \overline{[\Delta T(r)]^2} = 4C_{0,T}\langle\epsilon_T\rangle\langle\epsilon\rangle^{-1/3}r^{2/3}, \tag{6}$$

where $\Delta u(r) = u(x+r) - u(x)$, $\Delta w(r) = w(x+r) - w(x)$, and $\Delta T(r) = T(x+r) - T(x)$ are the velocity and temperature increments at separation distance (or scale) r; $\langle\epsilon\rangle$ and $\langle\epsilon_T\rangle$ are the k and temperature variance dissipation rates, respectively; $C_{0,u}$ and $C_{0,w}$ are the Kolmogorov constants for the longitudinal and vertical velocity components; and $C_{0,T}$ is the Kolmogorov-Obukhov-Corrsin (KOC) constant. These scaling laws, obtained under the assumptions of similarity and local isotropy, appear to hold reasonably in the ASL for scales smaller than $z/2$ [29]. Moreover, the normalized third-order structure functions

$$S(r) = \frac{S_u^3}{\left(S_u^2\right)^{3/2}} = \frac{\langle\Delta u(r)^3\rangle}{\langle\Delta u(r)^2\rangle^{3/2}} \tag{7}$$

and

$$F(r) = \frac{S^3_{TTu}}{S^2_T\left[S^2_u\right]^{1/2}} = \frac{\langle \Delta u(r)\Delta T(r)^2\rangle}{\langle \Delta T(r)^2\rangle\langle \Delta u(r)^2\rangle^{1/2}} \tag{8}$$

must be constant to recover Kolmogorov predictions for S^2_u and S^2_T in the inertial range [30].

However, relevant deviations from Kolmogorov scaling have been reported for higher-order structure functions, especially for the scalar fluctuations. These deviations arise as (i) Eqs. (4)–(6) do not account for intermittency related to spatial variability of the actual ϵ and ϵ_T and (ii) the hypothesis of local isotropy might not hold for scalars due to nonlocal interactions across scales [31]. A signature of the latter is the large structure skewness for temperature determined by ramp structures [4,29]. Many models, starting from Kolmogorov's log-normal dissipation rate refinement [32], seek to relax some of the restrictive assumptions of Kolmogorov so as to explain the anomalous scaling observed in higher-order moments. For scalars, these corrections are commonly expressed as

$$S^n_T = C_n(\epsilon r)^{n/3}(r/L_I)^{\zeta'_n - n/3}, \tag{9}$$

where the exponent ζ'_n implies a scaling different from Kolmogorov that depends on the moment order n. The presence of an integral timescale L_I suggests an explicit dependence on large-scale eddy motion within the inertial subrange. One estimate of L_I may be derived from the integral length scale of the flow given by

$$L_I = U I_w = U \int_0^\infty \rho_w(\tau_0) d\tau_0, \tag{10}$$

where $\rho_w(\tau_0)$ is the vertical velocity autocorrelation function and τ_0 is the time lag. Here I_w is presumed to be the most restrictive scale given that w' is the flow variable most impacted by the presence of the boundary.

The statistics of air temperature increments across scales (τ_0/I_w) for different ζ conditions are explored with a lens on two primary features: buildup of heavy tails and destruction of asymmetry originating from ramp-cliff structures at the crossover from $\tau_0/I_w > 1$ to $\tau_0/I_w \approx 0.1$. Because changes in ζ do result in changes in I_w, the time (or space) lags are presented in dimensionless form as $\tau = \tau_0/I_w$, so the increments of a flow variable Δs, with $\Delta s = \Delta u, \Delta w, \Delta T$ at a given dimensionless scale τ, can be expressed as $\Delta s(\tau) = s(t+\tau) - s(t)$, where $t = t_0/I_w$.

B. Probabilistic description of intermittency across scales

The intermittent behavior of ASL turbulent flows has been documented by several experiments [33,34] and a number of models have been proposed to capture the effects of intermittency on the flow statistics in the inertial range of scales (e.g., log-normal, bifractals, and multifractals to beta model, logarithmically stable, She-Leveque vortex filaments, etc). Common to all these models is the hypothesis of local isotropy and the accounting for uneven distribution of eddy activity in the space-time domain, which explains the anomalous scaling of higher-order even structure functions.

Here a statistical description of scalar increments is used to fingerprint large-scale signatures across scales τ for different ζ. If such fingerprints exist, the dissipation rates ϵ and ϵ_T need not be sufficient to describe all aspects of the inertial range statistics. The one-time probability density function (PDF) of the increments $\Delta s(\tau)$ of the flow variable $s = u, w, T$ at a given dimensionless scale τ can be expressed as [35]

$$p(\Delta s) = \frac{N}{q_0(\Delta s)} \exp \int_0^{\Delta s} \frac{r_0(\Delta s')}{q_0(\Delta s')} d\Delta s'. \tag{11}$$

This expression is exact when Δs are realizations of a stationary stochastic process $S(t)$ under the condition $p(\Delta s) \to 0$ as $\Delta s \to \infty$. Here $q_0(\Delta s) = \langle \dot{S}^2|\Delta s\rangle/\langle \dot{S}^2\rangle$ and $r_0(\Delta s) = \langle \ddot{S}|\Delta s\rangle/\langle \dot{S}^2\rangle$ are the normalized averages of the first- and second-order conditional derivatives of the process $S(t)$

and N is a normalization constant. Equation (11) generalizes previous results obtained by Sinai and Yakhot [36] and Ching [37] for the PDF of temperature fluctuations and their increments, where the term $r_0(\Delta s)$ was linear [$r_0(\Delta s) = -\Delta s$]. Equation (11), while derived for a twice-differentiable process, can be interpreted as the steady-state solution of a Fokker-Planck equation with $p(\Delta s)$ vanishing at infinite boundaries, with drift and diffusion coefficient equal to r_0 and q_0, respectively [38,39].

Although Eq. (11) can be directly computed from an observed time series, the estimation of the conditional derivatives in $q_0(\Delta s)$ and $r_0(\Delta s)$ becomes inevitably uncertain as Δs approaches the tails of the PDF. However, a number of parametric distributions commonly used in statistical mechanics arise as particular cases of Eq. (11) when $r_0(\Delta s) = -\Delta s$, such as Gaussian ($q_0$ constant), power laws [$q_0(\Delta s) \sim \Delta s^2$], and stretched exponentials [$q_0(\Delta s) \sim \Delta s^a$, $0 < a < 2$]. To facilitate estimation and comparisons with data, two different parametric models for the tails of Eq. (11) are here adopted: a stretched exponential (SE) and a q-Gaussian (QG) distribution. The first arises from multiplicative processes of normal-distributed random variates [40], while the second maximizes a generalized measure of information entropy proposed by Tsallis [41–43]. While QG does not have a clear physical basis in the context of turbulent flows [44], it has been widely used in the analysis of turbulence simulations and data [13,45–47]. We employ these two models to infer tail behavior as well as to test the independence of our findings from the particular parametric distribution used to characterize $p(\Delta s)$. The QG and SE PDFs are given as

$$p_{\mathrm{QG}}(\Delta s) = N(q)\left(1 + (q-1)\frac{\Delta s^2}{2\psi^2}\right)^{1/(1-q)}, \tag{12}$$

$$p_{\mathrm{SE}}(\Delta s) = \frac{\eta}{\lambda}\left(\frac{\Delta s}{\lambda}\right)^{\eta-1} \exp\left(\frac{\Delta s}{\lambda}\right)^{\eta}. \tag{13}$$

Both PDF models have two degrees of freedom corresponding to a scale (ψ and λ) and shape (η and q) parameter. We adopt the (symmetric) QG model and the SE fitted separately to right and left tails of $p(\Delta T)$.

C. Probabilistic description of asymmetry and irreversibility across scales

The presence of ramp-cliff structures has been conjectured to result in nonlocal interactions of different size eddies within the inertial subrange [4]. This nonlocality affects both even and odd moments of higher order. A statistical framework to investigate the effects of ramps on the asymmetric nature of velocity and scalar increments for different atmospheric stability classes is now discussed. Sharp edges associated with cliffs might directly inject scalar variance at much smaller scales and thus alter the magnitude and sign of odd-order moments within the inertial range (depending on z/L). The presence of asymmetry has been investigated based on odd-ordered structure functions [4] or multipoint correlators [48]. In particular, a simple measure for the persistence of asymmetry at small scales is the skewness of the scalar increments $S_T^3 = \langle \Delta T(\tau)^3 \rangle / \langle \Delta T(\tau)^2 \rangle^{3/2}$. The structure skewness of air temperature has been found to scale as $\mathrm{Re}_\lambda = \sigma_u \lambda / \nu$ (where λ is the Taylor microscale and σ_u is the root mean square of the longitudinal velocity fluctuations) and thus for a boundary layer $S_3^T \sim \mathrm{Re}_*^{1/2}$. However, for large values of Re_λ experimental evidence suggests that S_3^T tends to plateau and become independent of Re_λ [4,31].

A further signature of ramp-cliff structures is that increments $\Delta T(\tau)$ may exhibit a time-directional (or irreversible) behavior. Time reversibility implies that the trajectories of a stationary process Θ_t exhibit the same statistical properties when considered forward or backward in time. In particular, for a reversible time series the n-point joint PDF of $(\Theta_1, \Theta_2, \ldots, \Theta_n)$ is equal to the joint PDF of the reversed sequence $(\Theta_n, \Theta_{n-1}, \ldots, \Theta_1)$ for every n. While testing this general definition of reversibility would require perfect knowledge of the phase-space trajectories, a weaker definition is the so-called lag reversibility. This condition only requires the two-point PDFs to be

equal: $f_{\Theta_t,\Theta_{t+\tau}}(\Theta_1,\Theta_2) = f_{\Theta_{t+\tau},\Theta_t}(\Theta_2,\Theta_1)$. While this definition is less general, it still provides a necessary condition for testing time reversibility. Moreover, it is consistent with the traditional descriptions of turbulence that are primarily based on two-point statistics. Lag reversibility implies that [49]

$$R_\tau = \rho_c\left(\Theta_t^2, \Theta_{t+\tau}\right) - \rho_c\left(\Theta_t, \Theta_{t+\tau}^2\right) = 0, \tag{14}$$

where ρ_c denotes a correlation coefficient between two variables. This condition can be directly tested across different τ and ζ using a conventional correlation analysis.

A second test for reversibility of scalar trajectories is here performed based on the Kullback-Leibner measure, a form of relative entropy that determines the average distance between the entire PDF of forward and backward trajectories [39,50,51]. Again, the analysis here is restricted to the inspection of lag reversibility ($n = 2$) across scales τ. In such a restricted form, this measure reduces to

$$\langle Z_\tau \rangle = \int_{\Omega_\Theta}\int_{\Omega_{\Theta'_\tau}} p(\Theta'_\tau|\Theta)p(\Theta)\ln\frac{p(\Theta'_\tau|\Theta)}{p(-\Theta'_\tau|\Theta)}d\Theta'_\tau d\Theta, \tag{15}$$

where $\Theta'_\tau = \Delta\Theta(\tau)/\tau$, and the domains of integration Ω_Θ and $\Omega_{\Theta'_\tau}$ correspond to the populations of the random variables Θ and Θ'_τ, respectively. Equation (15) determines, at each dimensionless scale τ, the average distance between the probability of the transition $\Delta\Theta(\tau)$ and its inverse, at every given level Θ.

A statistical mechanics interpretation of Eq. (15) would imply that for a system in nonequilibrium steady state, the fluctuation theorem must hold so that

$$\ln\frac{p(-Z_\tau)}{p(Z_\tau)} = -Z_\tau \tag{16}$$

for the variable Z_τ computed at some level Θ,

$$Z_\tau(\Theta) = \ln\frac{p(\Theta'_\tau|\Theta)}{p(-\Theta'_\tau|\Theta)}. \tag{17}$$

Note here the usage of conditional probabilities instead of their unconditional forms employed in recent flight-crash studies of Lagrangian fluid particles [15] that also made use of fluctuation theorem and time reversibility. Equation (15) has been shown to have general validity [51] independent of the underlying dynamics or statistical-mechanics interpretations, when considering conditional statistics.

III. DATA AND METHODS

The three velocity components and air temperature measurements were sampled at 56 Hz using an ultrasonic anemometer positioned at $z = 5.2$ m above a grass-covered surface at the Blackwood Division of the Duke Forest, near Durham, North Carolina, USA. The anemometer samples the air velocity in three nonorthogonal directions by transmitting sonic waves in opposite directions and measuring their travel times along a fixed 0.15-m path length. Temperature fluctuations are then computed from measured fluctuations in the speed of sound, assuming air is an ideal gas. The nonorthogonal sonic anemometer design used here has proven to be the most effective at reducing flow distortions induced by the presence of the instrument.

The experiment resulted in 123 time-series records (henceforth termed runs), each having a duration of 19.5 min (65 536 data points at 56 Hz), covering a range of different atmospheric stability conditions [29]. Of these, only 34 runs passed a stationarity test and were included in the analysis (see Table I for a summary of the properties of the flow for these runs). The assumption of stationarity is necessary so as to (i) decompose the flow variables into a mean and fluctuating part, (ii) adopt Eqs. (11) and (15) so as to describe intermittency and time irreversibility respectively, and (iii) compute the integral scales needed in delineating the transition from production to inertial.

TABLE I. Bulk flow properties for the runs in our data set. The table reports the atmospheric stability parameter ζ, the Obukhov length L (in m), the sensible heat flux $H = \rho C_p \overline{w'T'}$ (in W m^{-2}) (where ρ is the mean air density and C_p is the specific-heat capacity of dry air at constant pressure), the mean air temperature T (in °C), the mean velocity U (in m/s), the integral timescale for w (in s), the turbulent intensity σ_u/U, the temperature standard deviation σ_T (in °C), and the vertical velocity standard deviation σ_w (in m/s).

Run	ζ	L	H	T	U	I_w	σ_u/U	u^*	σ_T	σ_w
1	−11.56	−0.4	93.2	33.9	2.1	2.62	0.44	0.08	0.48	0.40
2	−1.31	−4.0	121.6	26.9	1.0	7.58	0.72	0.17	0.54	0.30
3	−0.89	−5.8	73.1	27.8	0.5	6.62	0.91	0.16	0.37	0.30
4	−0.81	−6.4	79.9	32.7	0.7	5.75	1.05	0.17	0.61	0.29
5	−0.80	−6.5	138.1	27.4	0.8	8.18	0.48	0.21	0.57	0.31
6	−0.67	−7.7	149.8	31.4	0.9	11.64	1.04	0.23	0.63	0.38
7	−0.59	−8.8	118.1	34.8	1.5	3.43	0.71	0.22	0.58	0.34
8	−0.52	−10.0	85.4	32.5	2.1	1.74	0.37	0.21	0.44	0.37
9	−0.45	−11.5	78.6	31.7	1.1	7.44	0.61	0.21	0.43	0.30
10	−0.44	−11.7	110.7	31.9	1.2	5.89	0.65	0.24	0.49	0.37
11	−0.44	−11.8	39.4	34.4	1.3	3.19	0.45	0.17	0.32	0.29
12	−0.40	−13.0	36.6	34.1	1.7	2.30	0.39	0.17	0.37	0.28
13	−0.37	−14.0	65.1	25.2	1.6	2.91	0.39	0.21	0.35	0.27
14	−0.33	−15.6	48.0	28.9	1.4	2.58	0.41	0.20	0.27	0.30
15	−0.33	−15.8	4.8	33.4	1.6	1.59	0.35	0.09	0.09	0.23
16	−0.29	−18.2	115.2	32.1	2.7	2.16	0.37	0.28	0.44	0.47
17	−0.28	−18.5	136.2	29.2	0.9	6.88	1.11	0.30	0.56	0.37
18	−0.27	−19.1	108.6	30.5	1.7	3.56	0.62	0.28	0.54	0.34
19	−0.17	−29.7	70.5	29.5	2.6	2.22	0.29	0.28	0.36	0.42
20	−0.15	−33.8	63.2	32.9	2.2	2.97	0.39	0.28	0.36	0.40
21	−0.14	−37.9	30.9	34.2	1.6	4.17	0.49	0.23	0.34	0.32
22	−0.12	−44.4	118.6	31.0	2.6	3.78	0.42	0.38	0.49	0.42
23	−0.09	−56.5	26.7	33.9	1.9	3.39	0.31	0.25	0.15	0.31
24	−0.08	−61.7	49.7	31.7	2.0	3.50	0.41	0.31	0.27	0.39
25	−0.08	−65.1	17.6	34.0	2.2	3.22	0.29	0.23	0.13	0.31
26	−0.07	−72.5	28.8	31.5	1.8	2.71	0.41	0.28	0.29	0.30
27	−0.04	−126.2	45.1	31.0	4.3	1.21	0.33	0.39	0.35	0.71
28	−0.03	−171.8	3.9	31.3	1.7	3.18	0.39	0.19	0.15	0.30
29	−0.02	−261.4	46.1	31.2	3.8	1.37	0.39	0.50	0.23	0.72
30	−0.02	−304.3	47.1	29.4	5.0	0.84	0.31	0.53	0.21	0.80
31	0.002	2397.4	−0.4	31.2	1.9	1.94	0.44	0.22	0.69	0.32
32	0.01	525.5	−1.3	32.9	0.9	3.00	0.51	0.19	0.18	0.23
33	0.05	93.8	−20.7	29.8	2.6	1.52	0.30	0.27	0.23	0.39
34	0.07	71.4	−14.2	30.4	1.9	2.18	0.37	0.22	0.25	0.28

To test the data set for stationarity, we employ the second-order structure functions of velocity components (u and w) and air temperature T. Runs were included only if the slope of $S_s^2 = \langle [s(t+\tau) - s(t)]^2 \rangle$ for time delays larger than about 9 min (30 000 sample points) was smaller than a fixed value (0.01). For the 34 runs meeting this strict stationarity criterion, second-order structure functions for w and T are featured in Fig. 1. As expected, structure functions exhibit an approximate 2/3 scaling at fine scales and transition to a constant value as the autocorrelation weakens at large separation distances.

The presence of a stable stratification is known to produce distortions on the spectral properties of turbulence at scales commensurate with (and larger than) the Dougherty-Ozmidov length scale [52]. We investigated this issue (see the Appendix for more details), finding that stable stratification

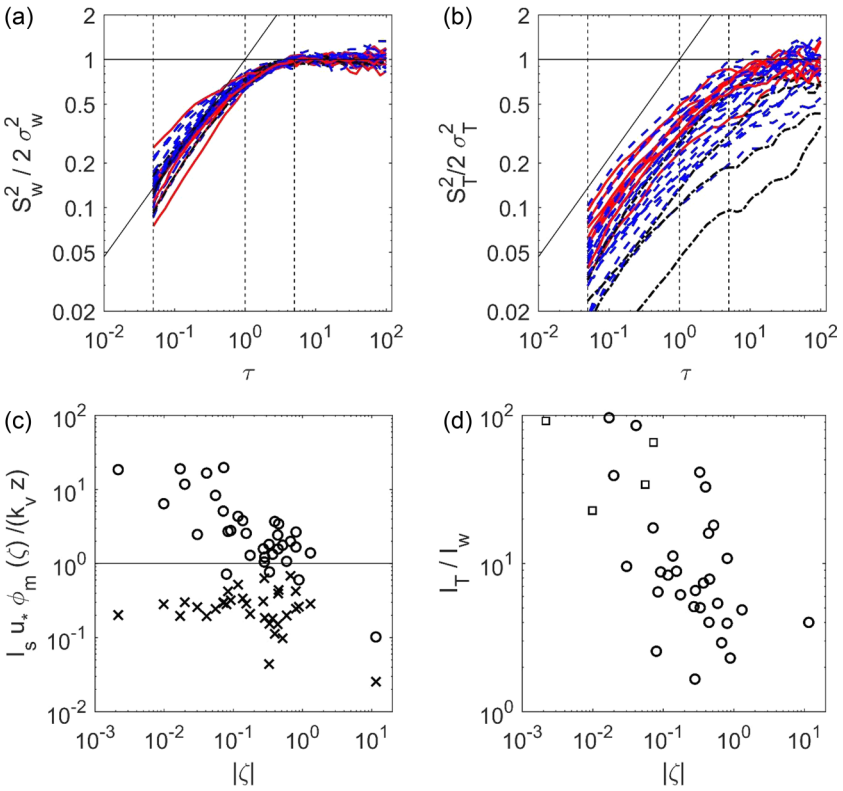

FIG. 1. Normalized second-order structure functions for (a) vertical velocity and (b) temperature are shown for runs that are weakly unstable (blue dashed lines), strongly unstable (red solid lines), and stable (black dash-dotted lines). Black lines indicate the value 1 and the 2/3 power law for reference; vertical dashed lines correspond to the dimensionless scales $\tau = 0.05$ (smallest scale not impacted by instrument path length), $\tau = 1$ (integral scale of the flow), and $\tau = 5$ (typical scale larger than I_w, while small enough not to be impacted by statistical convergence issues in structure functions calculations). (c) Integral scales of the flow for $s = T$ (circles) and $s = w$ (crosses) as a function of the stability parameter $|\zeta|$ and (d) their ratio I_T to I_w again as a function of $|\zeta|$, where stable runs ($\zeta > 0$) are indicated by black squares.

effects are only relevant at scales larger than the integral scale I_w considered here and not in the inertial range.

As earlier noted, the most restrictive (i.e., smallest) integral timescale is I_w associated with the vertical velocity w due to ground effects. We assume that this timescale characterizes the transition from production to inertial ranges for all three flow variables u, w, and T. Equation (10) is here evaluated by integrating $\rho_w(\tau)$ up to the first zero crossing so as to avoid the effects of low-frequency oscillations. Figure 1 illustrates the integral timescales of w and T as a function of ζ, where the aforementioned integral timescales are normalized by the mean vorticity timescale $dU/dz = \phi_m(\zeta)u_*(\kappa_v z)^{-1}$. It is clear that such normalized I_w is approximately constant across stability regimes and suggests I_w to be proportional to the duration of vortices most efficient at transporting momentum to the ground for all ζ. Conversely, the temperature integral timescale is much longer than I_w for near-neutral conditions and only approaches I_w for strongly unstable conditions.

A known limitation of sonic anemometry is the presence of distortions at high frequencies due to instrument path averaging. For this reason, the smallest timescale considered in the analysis is $0.05I_w$, which corresponds to a minimum travel path of 30 cm (or twice the sonic anemometer path length). Taylor's frozen turbulence hypothesis [53] ($r = -\overline{U}t$) was employed to convert values of

τ to separation distances r within the inertial subrange even though the turbulent intensity σ_u/U is not small as shown in Table I. For this reason, we adopt the dimensionless lag τ for analysis and presentation. The τ can be interpreted as temporal or spatial, noting that distortions due to the use of Taylor's hypothesis impact similarly the numerator and denominator.

For every run, ζ was computed using Eq. (3) and then employed to classify the ASL stability condition. Most of the runs in the data set are unstable with a wide range of $|\zeta|$, while only four runs are characterized by $\zeta > 0$. To ensure a balanced statistical design, two stability classes are selected with the same number of runs (8) in each class: strongly unstable ($|\zeta| > 0.5$) and near-neutral runs ($|\zeta| < 0.072$). A summary of the bulk flow properties for these runs is featured in Table I.

In the analysis, each flow variable s ($s = u, w, T$) is normalized to zero mean and unit variance (labeled as s_n). Then, at scale τ, a time series of $\Delta s(\tau) = s_n(t+\tau) - s_n(t)$ is constructed and again normalized to have unit variance.

For illustration purposes, Fig. 2 shows sequences of fluctuations u', w', and T' extracted from runs in unstable and stable atmospheric regimes. In the first case, temperature fluctuations clearly exhibit ramp-cliff structures occurring with timescales larger than I_w. In the stable or near-neutral case, large-scale scalar structures are still present even though their structure is qualitatively different from the unstable case and may include inverted ramp structures as in Fig. 2(b) when $\overline{w'T'} < 0$.

To test the effects of these coherent structures on inertial subrange statistics and in particular to isolate the effect of temperature ramps on intermittency and asymmetry, synthetic time series are used and are constructed as follows. First, a phase randomization of the original temperature records [54] is performed by preserving the amplitudes of the Fourier coefficients while destroying coherent patterns encoded in the phase angle. A synthetic sawtooth time series is then superimposed on the time series obtained by phase randomization. Here a coefficient α measures the relative weight of the ramps with respect to the phase-randomized sequence. This combination yields realizations of a renewal process [see Fig. 2(c) for a representative example with $\alpha = 0.5$] that is unconnected with Navier-Stokes scalar turbulence, but mimics sweep-ejection dynamics [13]. Synthetic ramps are here generated with exponentially distributed durations and with a mean duration set to a multiple of the integral timescale [$2I_w$ in Fig. 2(c)]. The resulting time series is again normalized to have zero mean and unit variance.

IV. RESULTS

The main questions to be addressed here require determination of (i) the probability of extreme scalar concentration excursions and concomitant intermittency and (ii) scalar asymmetry and time irreversibility across scales. Here tools introduced in Secs. II B and II C are used to investigate how these two features vary from production to inertial scales for temperature traces and to compare this behavior with the observed velocity components. Comparison of these quantities for runs recorded in different atmospheric stability conditions allows us to test whether significant coupling across scales exists and to what extent velocity and temperature statistics are universal at the smallest scale examined here.

A. Probabilistic description of intermittency across scales

We first investigate the intermittent behavior of both scalar and velocity components by assessing to what extent the scaling of even-order structure functions departs from Kolmogorov predictions. Inspection of scaling exponents ζ_n' in Eq. (9) for u, w, and T confirms that Kolmogorov predictions significantly overestimate scaling exponents for structure functions of order higher than 2, as shown in Fig. 3(a). The scaling exponents obtained for the scalar T show reasonable agreement with previous experimental results [Fig. 3(b)], with values systematically lower than predicted by the Kraichnan model in the limiting case of a time-uncorrelated velocity field [58]. The values of ζ_n' averaged over the set of runs observed during the experiment are lower for the scalar, especially

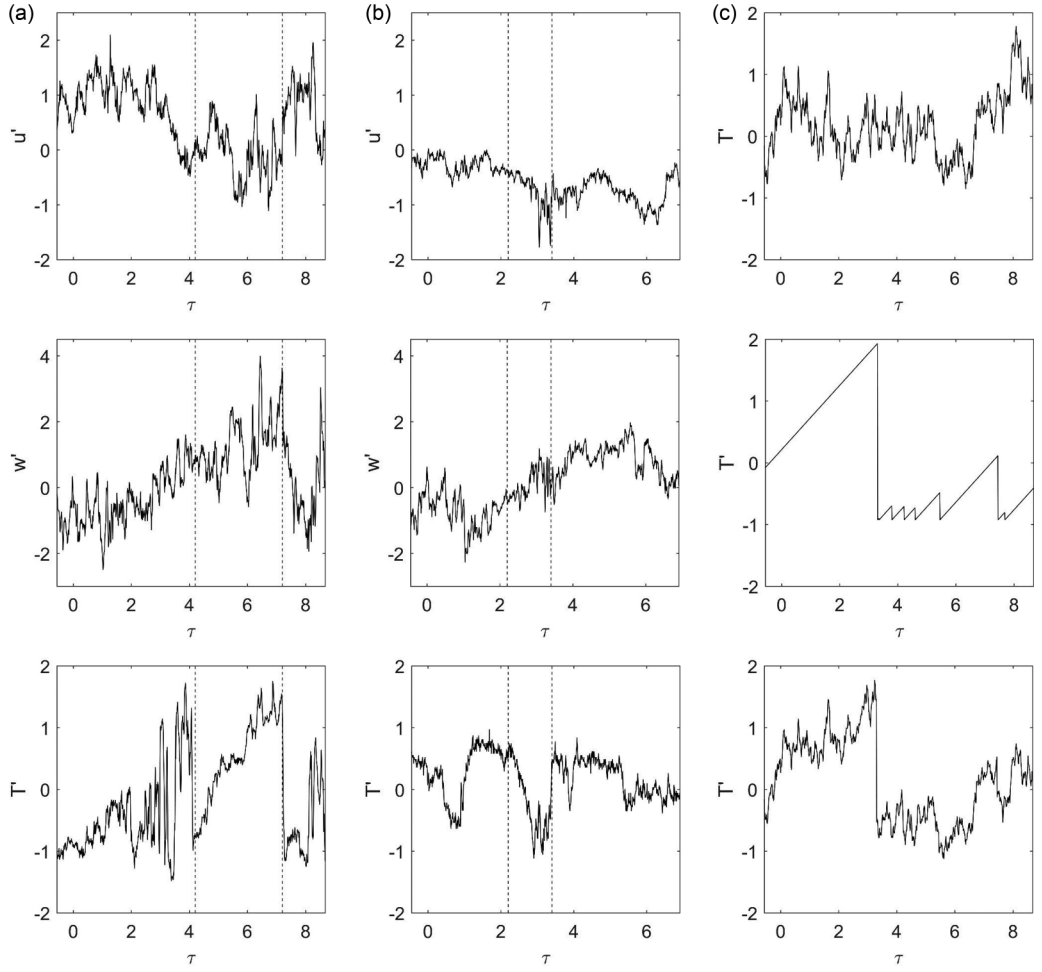

FIG. 2. Sequences of velocity and temperature fluctuations extracted from a strongly unstable run [run 8, $\zeta = -0.52$, $I_w = 1.74s$, column (a)] and a stable or near-neutral one [run 34, $\zeta = 0.07$, $I_w = 2.18s$, column (b)]. The presence of ramps and inverted-ramplike structures, respectively, is marked by dashed vertical lines. Column (c) illustrates a phase-randomized sequence obtained from run 34 (top), a series of synthetic ramps with durations exponentially distributed with mean $2I_w$ (middle), and the surrogate time series obtained merging the above sawtooth pattern with the phase-randomized time series (bottom), where the relative weight of the ramps α was set equal to 0.5.

when compared to the longitudinal velocity components. From this analysis, intermittency effects appear stronger for the scalar than for the longitudinal velocity.

The empirical PDFs of velocity and air temperature increments ($\Delta s = \Delta u, \Delta w, \Delta T$) for runs in the near-neutral ($|\zeta| < 0.072$) and strongly unstable ($\zeta < -0.5$) classes (Fig. 4) show clear transitions from a quasi-Gaussian regime at large lags ($\tau = 2$ in the figure) to distributions with sharper peaks and longer tails at scales well within the inertial subrange ($\tau = 0.05$). This behavior has been documented for a wide range of turbulent flows [59] and is associated with the buildup of intermittency [32] due to self-amplification inertial dynamics [60].

The bulk of the PDF of temperature increments at any given scale can also be characterized by the coefficients of Eq. (11). Results show some differences between runs with differing $|\zeta|$ (Fig. 5). Namely, for runs in the strongly unstable class, q_0 exhibits a more pronounced peak

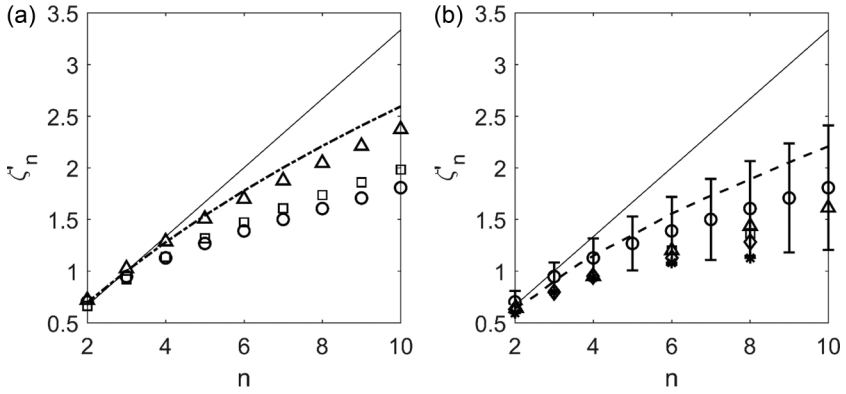

FIG. 3. (a) Average values of the scaling exponents for longitudinal velocity u (triangles), vertical velocity w (squares), and temperature T (circles). Black solid lines and dashed lines show, respectively, the Kolmogorov and the She-Leveque predictions for the longitudinal velocity structure functions. Exponents are computed from scales ranging between $\tau = 0.05$ and $\tau = 0.2$. (b) Scaling exponents for temperature only; Mean and standard deviation values are computed over all the runs and are indicated by circles and vertical bars, respectively. Data from Mydlarsky and Warhaft [61] (squares), Antonia *et al.* [55] (triangles), Meneveau *et al.* [56] (asterisks), and Ruiz-Chavarria *et al.* (diamonds) [57] are shown for comparison. The KOC scaling (black line) and results from the Kraichnan model [58] (dashed line) as reported in [4] are also presented for reference.

around the origin and is characterized by larger asymmetry at the crossover scale $\tau = 1$ compared to their near-neutral counterparts [Fig. 5(a)]. Moreover, the results here confirm that a choice of linear $r_0(\Delta T)$ and quadratic $q_0(\Delta T)$ appears reasonable for ASL flows. In the case of an unstable

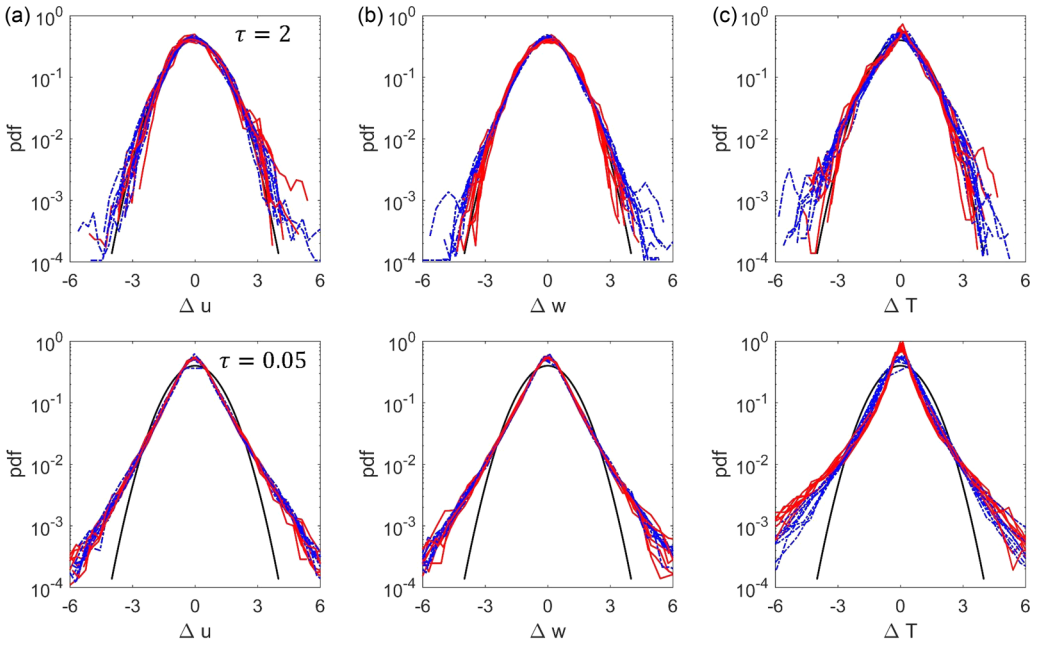

FIG. 4. Normalized probability density functions observed for increments of (a) longitudinal velocity, (b) vertical velocity, and (c) air temperature at large scales ($\tau = 2$, top panels) and small scales ($\tau = 0.05$, bottom panels). The figure includes data from runs in the strongly unstable class ($\zeta < -0.5$, shown in red) and near-neutral class ($|\zeta| < 0.072$, blue). Black lines show the standard Gaussian distribution for reference.

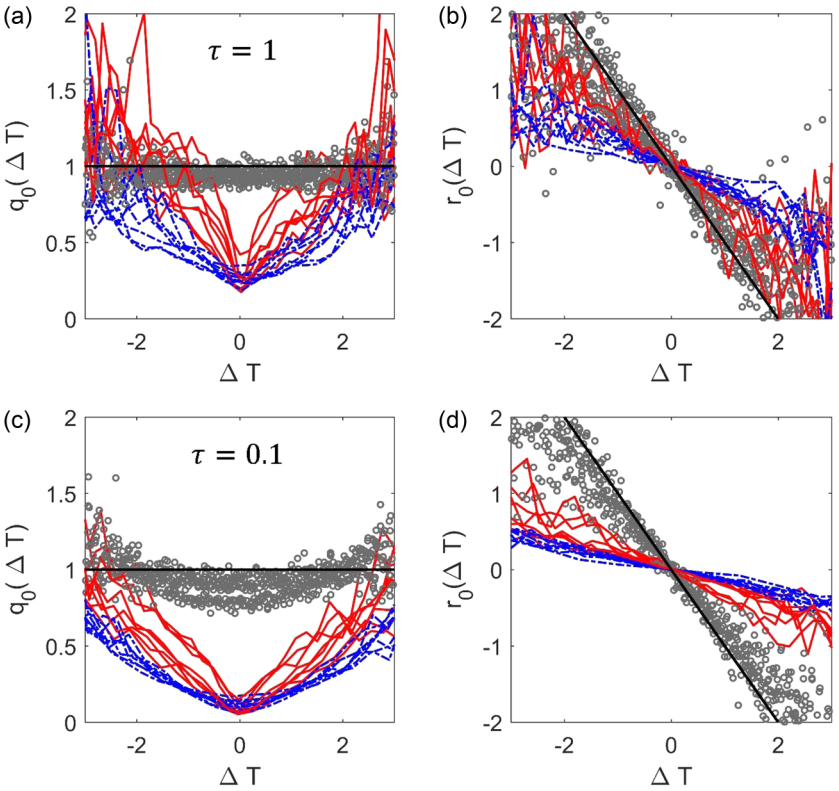

FIG. 5. Functions $q_0(\Delta T)$ and $r_0(\Delta T)$ estimated from the conditional derivatives of the original temperature time series, for the two classes of strongly unstable (red solid lines) and near-neutral runs (blue dashed lines). The same quantities are reported for phase-randomized surrogate time series for comparison (gray circles). Results are shown for the central body of the PDF (within 3σ from the mean) for illustration purposes. Results are computed for (a) and (b) a lag equal to the integral timescale of the flow $\tau = 1$ and (c) and (d) the smaller time lag $\tau = 0.1$. Black lines $q_0 = 1$ and $r_0 = -\Delta T$ correspond to the standard Gaussian distribution.

ASL, the term $r_0(\Delta T)$ remains linear, while inspection of $q_0(\Delta T)$ suggests that a dependence on s with an exponent smaller than 2 might be more appropriate, corresponding to stretched exponential tails for $p(\Delta T)$ for small lags τ in unstable ASL flows. Comparison with the same data after run-by-run spectral phase randomization [54] shows that the latter exhibits almost Gaussian behavior, confirming that the emergence of long tails at inertial scales is primarily a consequence of nonlinear structures in the original time series.

The variation of the tail parameters $\boldsymbol{\eta}$ and q with decreasing scale τ (Fig. 6) provides a robust measure of how the distributional tails of $p(\Delta T)$ evolve at the onset of the inertial range. For temperature differences, the rates of change across scales of both η and q appear to be dependent on the magnitude of the stability parameter ζ. Consequently, while at large scales, where the PDF closely resembles a Gaussian, neither $\boldsymbol{\eta}$ nor q exhibits a significant dependence on ζ, for scales well within the inertial subrange stability is clearly impacting the tail behavior of ΔT (Fig. 7).

This evidence suggests that the observed intermittency not only is internal (i.e., not only due to variability in the instantaneous dissipation rate [9]) but is also directly impacted by the larger-scale eddy motion that senses boundary conditions. In particular, when buoyancy generation is significant, the heat flux $\overline{w'T'}$ is connected with the sweep and sudden ejection of air parcels, corresponding to the sharp edges of the temperature ramps [3,13]. The resulting sawtooth behavior could be responsible for the injection of scalar variance at small scales (instead of a gradual cascade), acting

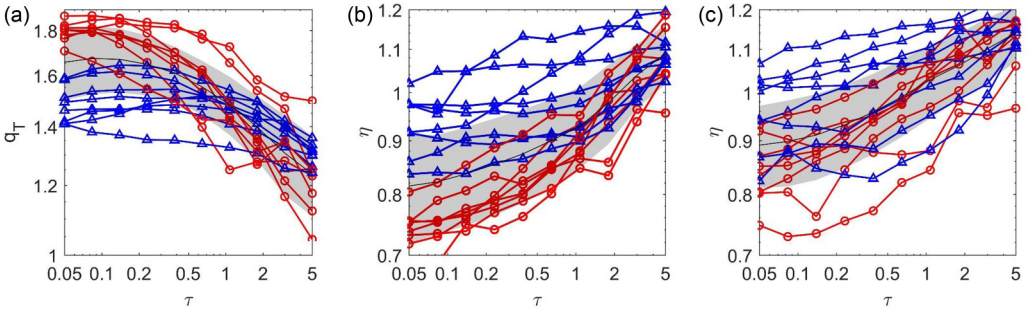

FIG. 6. Evolution across scales τ of (a) the q-Gaussian tail parameter q, and of the stretched exponential shape parameter η obtained from a separate fit to the (b) left and (c) right tails of the distribution of temperature increments. Data from two stability classes are included: strongly unstable ($\zeta < -0.5$, red circles) and near-neutral conditions ($|\zeta| < 0.072$, blue triangles). Black lines and shaded areas indicate average values and standard deviations, respectively, computed over the entire data set.

in particular on the negative tail of the ΔT PDF, as evident from Fig. 5(a). On the other hand, the buildup of non-Gaussian statistics for velocity increments is not as impacted by the stability regime and therefore the dominant effects are in this case primarily an effect of internal intermittency.

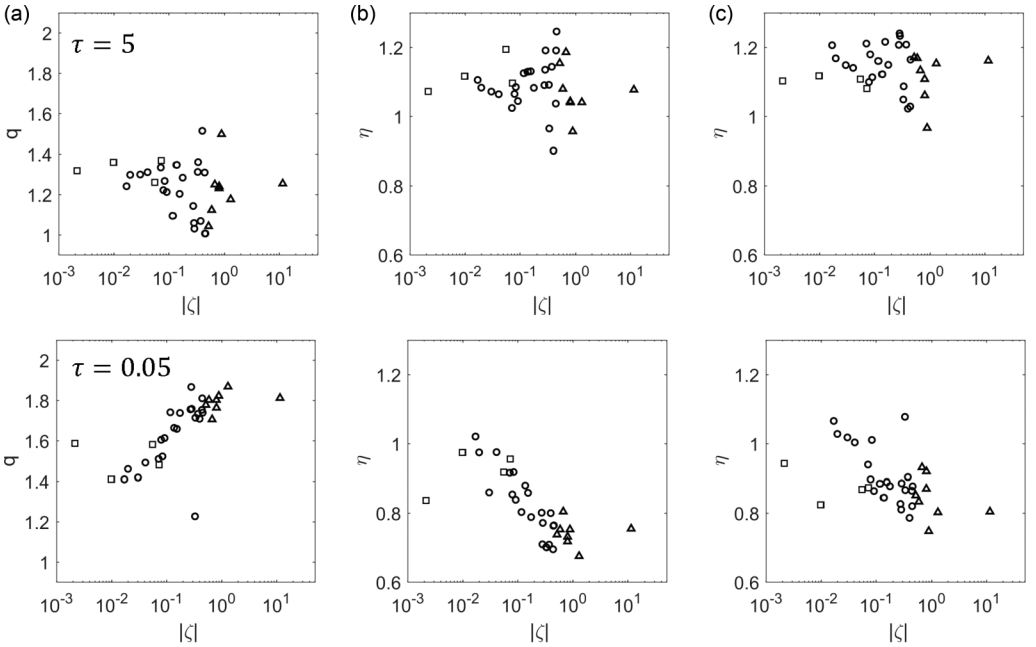

FIG. 7. Tail parameters of the PDF of temperature increments across stability conditions ζ. Results include the q-Gaussian tail parameter q [column (a)] and the stretched exponential shape parameter η, obtained from fitting the left [column (b)] and right [column (c)] tails of the distribution $p(\Delta T)$. Values of q and η are reported for large scales ($\tau = 5$, top panels) and small scales ($\tau = 0.05$, bottom panels). Triangles denote strongly unstable runs ($\zeta < -0.5$), squares denote stable runs ($\zeta > 0$), and circles refer to slightly unstable runs ($-0.5 < \zeta < 0$).

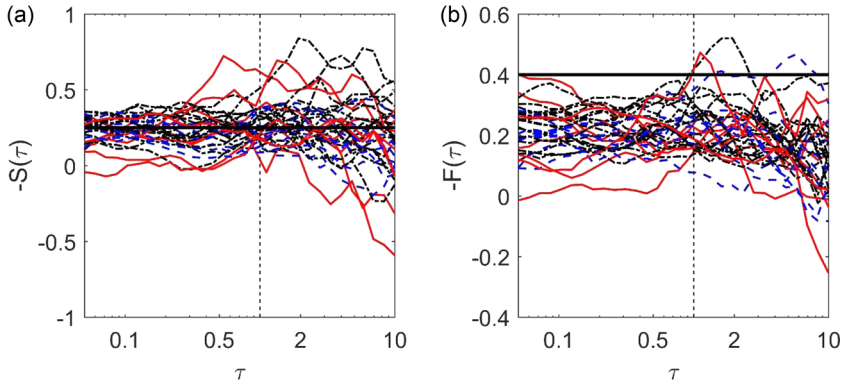

FIG. 8. Normalized third-order structure functions $S(\tau)$ and $F(\tau)$ at the crossover from inertial to production scales. Vertical dashed lines indicate the integral timescales and horizontal solid lines show the constant values (a) 0.25 and (b) 0.4. Results are shown for near-neutral runs ($|\zeta| < 0.072$, blue dashed lines), strongly unstable runs ($|\zeta| > 0.5$, red solid lines), and runs with intermediate values of $|\zeta|$ (black dash-dotted lines).

B. Probabilistic description of asymmetry across scales

To compare the data sets used here with laboratory studies, we first test the validity of Obukhov's constant skewness hypothesis, which would require the third-order structure function of the longitudinal velocity component being constant within the inertial range. Figure 8 reports the values of the third-order structure functions (7) and (8) evaluated at the onset of the inertial subrange as delineated by the w time series. Both are approximately constant for scales smaller than I_w. While comparison with experiments shows good agreement for $S(\tau) \simeq -0.25$, $F(\tau)$ is systematically smaller than its anticipated value [29] (-0.4) for all ζ.

For the scalar T, the presence of a finite third-order temperature structure function signifies that local isotropy is not fully attained in the range of scales explored here. The temperature skewness S_T^3 exhibits a plateau for scales smaller than I_w [Fig. 9(a)] similar to previous measurements reported

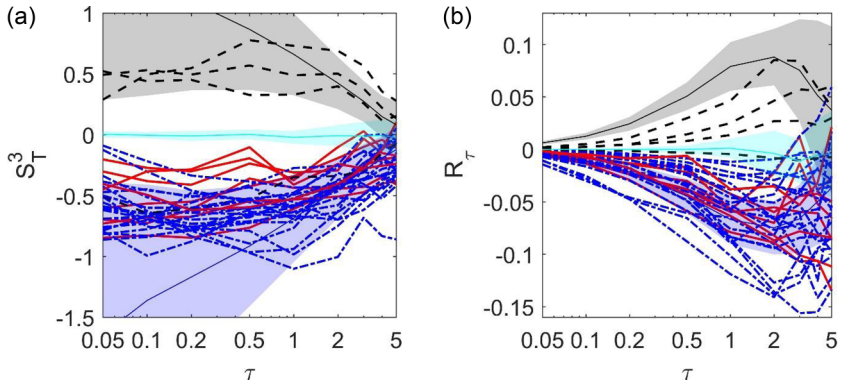

FIG. 9. Measures of (a) asymmetry S_T^3 and (b) time irreversibility R_τ computed for temperature increments for scales varying from $\tau = 0.05$ to $\tau = 5$. The plots include stable runs (black dashed lines), weakly unstable runs (blue dash-dotted lines), and strongly unstable runs (red solid lines). For reference, the same quantities are computed for phase-randomized time series (cyan) and synthetic time series with sawtooth positive (blue) and inverted (black) ramps. Shaded regions correspond to the 1σ-confidence intervals over 34 realizations of the surrogate time series. The relative weight and mean duration of the synthetic ramps were set to $\alpha = 0.4$ and $2I_w$, respectively.

in grid turbulence forced by a mean temperature gradient [61]. Moreover, S_T^3 levels off to positive values for $\zeta > 0$, while it becomes negative for $\zeta < 0$. This finding is consistent with the presence of ramplike structures when $\zeta > 0$ (mildly stable conditions) that are inverted when compared to their unstable counterparts.

The findings here confirm that at the crossover from production to inertial, imprints of ramp structures persist well into the inertial subrange. The consequence of these imprints on time reversibility is now considered for temperature sequences. The irreversibility analysis detects strong irreversibility at large scales that slowly decreases at the onset of the inertial range (Fig. 9). This finding is consistent with the idea that atmospheric stability determines a preferential direction for the large-scale scalar structures, which becomes progressively weaker at scales smaller than $\tau = 1$. Here the sign of the heat flux has a primary effect on the orientation of the ramps, as captured by R_τ. Furthermore, phase randomization is shown to destroy much of this time irreversibility [Fig. 9(b)], while the addition of synthetic ramps, either with positive or negative orientation, produces values of R_τ that closely resemble observations of stable and unstable ASL, respectively. These synthetic experiments also recover the sign of the third-order moment S_T^3 [Fig. 9(a)], but not its magnitude at smaller scales. As one would expect, a sawtooth time series does not fully reproduce inertial scale scalar dynamics, even though it does clearly capture the qualitative effect of boundary conditions on scalar ramp-cliff structures.

Additional insight can be obtained by the relative entropy measure defined in Eq. (15), which was here evaluated by integrating the relative entropy over the joint frequency distribution of normalized temperature fluctuations and their increments at each scale τ. We used a coarse binning for estimating the joint PDF $p(T'(\tau), T)$ and assumed [51] that only finite probability ratios contribute to $\langle Z_\tau \rangle$. To check the consistency of this approach, calculations of Eq. (15) were repeated using a phase-space reconstruction technique based on embedding sequences $(T_t, T_{t+\tau})$ with delay time τ and embedding dimension 2, which confirmed the validity of this approach (results not shown).

The averaged relative entropy $\langle Z_\tau \rangle$, while insensitive to the ramp orientation, at every given level T quantifies the imbalance between forward and backward probability fluxes of temperature trajectories [Fig. 10(a)]. Again, irreversibility of scalar records increases with the lag τ and here tends to plateau at larger scales ($\tau > 1$).

Phase-randomized time series, by comparison, exhibit smaller values of $\langle Z_\tau \rangle$ in the inertial range. As one would expect, the excess is thus likely a direct result of the presence of scalar ramps. The presence of asymmetric patterns in temperature time traces further suggests that in the inertial range scalar turbulence is more time irreversible than velocity, as confirmed by the larger values of $\langle Z_\tau \rangle$ at inertial scales [Fig. 10(b)].

Time irreversibility of phase-space trajectories was further investigated by testing if a significant difference exists between the probability distributions $p(T'_\tau|T)$ and $p(-T'_\tau|T)$. To this end, a Kolmogorov-Smirnov (KS) test was performed at the significance level 0.05. At every scale τ, results were averaged over different values of T and across runs within the same stability class. The results from the KS test confirm the picture obtained from the relative entropy measure $\langle Z_\tau \rangle$: The PDF of forward and backward temperature diverges significantly as the scale τ increases as shown in Figs. 10(c) and 10(d). While this test does not capture the sign of the ramps, the behavior of near-neutral runs exhibits some difference from the case of relevant heat flux: Near-neutral runs appear on average more reversible than unstable runs at the same dimensionless scale τ.

V. DISCUSSION AND CONCLUSION

In this work, statistical measures for the frequency of extreme fluctuations and the time-directional behavior of observed time series were applied to scalar turbulence in the ASL. It was demonstrated that (i) the extreme value properties of the scalar markedly depend on the external forcing and (ii) scalar dynamics is characterized by time-irreversible behavior at the scales of injection of scalar variance in the turbulent flow. This time irreversibility propagates down to the

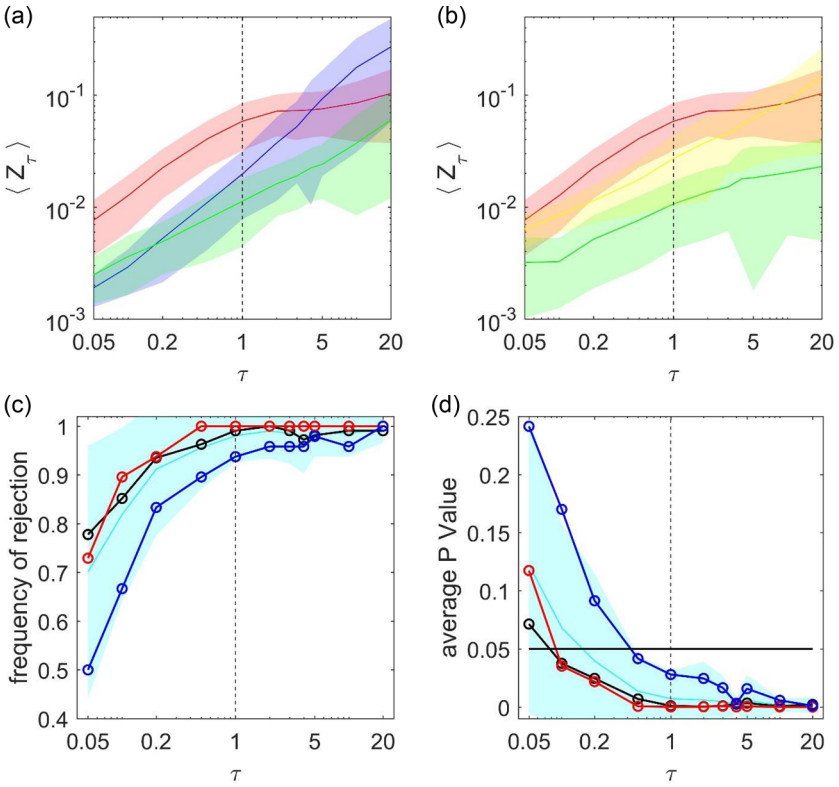

FIG. 10. (a) Mean and standard deviation over 34 time series of $\langle Z_\tau \rangle$ computed for scales varying from $\tau = 0.05$ to $\tau = 20$. Values of $\langle Z_\tau \rangle$ are shown for original temperature records (red) and surrogate time series obtained by phase randomization (green). For comparison, the same analysis is reported for fractional Brownian motion with Hurst exponent $H = 1/3$ (blue). (b) Comparison of $\langle Z_\tau \rangle$ for temperature (red), longitudinal velocity (yellow), and vertical velocity (green). Also shown are the (c) Kolmogorov-Smirnov test average rejection rate and (d) average P value computed for all the temperature time series (cyan for mean value and 1σ-confidence interval) and for different stability classes: strongly unstable runs ($\zeta < -0.5$, red), near-neutral runs ($|\zeta| < 0.072$, blue), and intermediate values ($0.072 < |\zeta| < 0.5$, black). The KS test was performed at the 0.05 significance level, corresponding to the horizontal line in (d). The vertical dashed line marks the integral timescale I_w.

smaller scales of the flow examined here, thus carrying the fingerprint of the energy injection mechanism.

It is well known that the PDFs of scalar increments develop heavier tails with decreasing scales in the inertial range when compared to their velocity counterparts. The analysis here shows that within the first two decades of the inertial subrange, this buildup of tails also carries the signature of turbulent kinetic energy generation. The direct injection of scalar variance from large scales seems to hinder any universal description of ΔT statistics within this range of scales. Instead, the PDF of $\Delta T(r)$ for ASL flows appears to be conditional on the value of ζ at scale r. This finding reinforces previous experimental results [62] obtained for a different type of flow (turbulent wake). In this case, the scalar injection mechanism was shown to impact higher-order scaling exponents of the temperature structure functions.

This dependence on atmospheric stability regime for $p(\Delta T)$ further suggests that the topology of large eddies, and in particular the presence of ramp-cliff scalar structures, may be responsible for the scalewise evolution of intermittency and the persistent time directionality at fine scales. This intermittency excess observed in the transition from production to inertial scales is consistent with

self-amplification dynamics taking place that further excites the excess of scalar variance injected by the ramps.

However, while measures of intermittency appear to be dependent on the absolute value of ζ, i.e., on the relative magnitude of shear and buoyancy production terms (regardless of the sign of the heat flux), the analysis of asymmetry and time reversibility clearly senses the sign of the heat flux H more than the magnitude of ζ itself. This effect is arguably a product of the preferential orientation that the external temperature gradient imposes on the scalar ramp-cliff structures, as explained by sweep-ejection dynamics. This hypothesis was here further tested by comparisons with synthetic time series that mimic ramp-cliff patterns observed in the scalar time series. The analysis confirmed that much of the observed time irreversibility, as well as its dependence on the sign of H, is recovered by these surrogate time series (Fig. 9).

The analysis of time-directional properties showed that time-irreversible behavior for the scalar is stronger at the large scales of the flow where boundary conditions, and in particular the sign of H, determine the orientation and structure of the eddies. At finer scales, time irreversibility as quantified by both $\langle Z_\tau \rangle$ and R_τ progressively decreases as advection destroys the preferential eddy orientation imposed by boundary conditions. Note that this behavior is not captured by a simple measure of skewness such as S_T^3 [Fig. 9(a)], which is small at large scales and plateaus in the inertial range consistent with previous experiments [4] and numerical simulations [63], thus showing that local isotropy is not fully attained at the finer scales examined here.

Turbulent flows exist in a state far from thermodynamic equilibrium, with the flow statistics exhibiting irreversibility. This irreversibility is typically described in terms of fluxes of energy or asymmetries in the PDFs of the fluid velocity increments [64]. Similar methods could be used to describe irreversibility in the scalar field, e.g., using S_T^3, and this would imply that the irreversibility of the scalar field is stronger at smaller scales than it is at larger scales. However, in this paper we have used alternative measures to quantify the irreversibility, namely, $\langle Z_\tau \rangle$ and R_τ. These quantities paint a different picture, namely, that it is the largest scales, not the smallest (inertial) scales in the scalar field, that exhibit the strongest irreversibility. A potential cause for these differing behaviors is that, whereas fluxes and quantities such as S_T^3 are multipoint single-time quantities, $\langle Z_\tau \rangle$ and R_τ are single-point multitime quantities. Thus, these two ways of describing irreversibility provide different perspectives about the nature of irreversibility in turbulence, which involves fields that evolve in both space and time. This difference in perspectives is a topic for future inquiry.

Collectively, the results presented in this paper suggest the following picture for ASL turbulence at the crossover from production to inertial. Increasing instability in the ASL leads to increases in the mean turbulent kinetic energy dissipation rate [as evidenced by Eq. (1)] and its spatial autocorrelation function and PDF. The consequences of this increased dissipation with increased instability have different outcomes for velocity and scalar turbulence. For velocity, refinements to Kolmogorov appear sufficient to explain the observed scaling in the inertial subrange. For scalar turbulence, the picture appears more complicated. Intermittency buildup with decreasing (inertial) scales is more rapid when compared to their velocity counterparts, and the signature of the temperature variance injection mechanism persists at even the finer scales explored here.

Turbulence and scalar turbulence are characterized by a constant flux of energy and scalar variance from the scales of production down to dissipation. While early theories hypothesized a cascade only depending on these quantities, experimental evidence to date supports a more complicated picture. The multitime information encoded in $\langle Z_\tau \rangle$ reveals that time reversibility is not constant across scales, as are the fluxes of information entropy. Probability fluxes forward and backward in time are not balanced in general for air temperature increments, especially at the crossover from production to inertial. Furthermore, these fluxes carry the signature of the external boundary conditions (i.e., H) and show that dissipation rates themselves are not independent of the large-scale dynamics. Although a formal analogy between Eq. (15) and the thermodynamics of microscopic nonequilibrium steady-state systems exists, we stress that in the present application turbulent fluctuations are macroscopic and are the result of nonlinear and nonlocal interactions.

ACKNOWLEDGMENTS

E.Z. acknowledges support from the Division of Earth and Ocean Sciences, the Nicholas School of the Environment at Duke University, and from the National Aeronautics and Space Administration (NASA Earth and Space Science Fellowship Grant No. 17-EARTH17F-270). G.K. acknowledges support from the National Science Foundation (Grants No. NSF-EAR-1344703, No. NSF-AGS-1644382, and No. NSF-DGE-1068871) and from the Department of Energy (Grant No. DE-SC0011461). We wish to thank Marco Marani, Brad Murray, and Amilcare Porporato for useful discussions and two anonymous reviewers whose comments improved the quality of the manuscript.

The authors declare no conflict of interest.

APPENDIX: STABLE STRATIFICATION AND DISTORTIONS OF THE INERTIAL SUBRANGE

In general, stable stratification limits the onset and extent of the inertial subrange given its damping effect in the vertical direction [52]. Here we show that the scales for which these effects are relevant occur at scales larger than the inertial range examined here. The Ozmidov length scale [65] (originally suggested by Dougherty [66]) is defined as the scale above which buoyancy forces significantly distort the spectrum of turbulence.

This length scale, sometimes labeled the Dougherty-Ozmidov scale, can be expressed as

$$L_0 = \sqrt{\frac{\epsilon}{N^3}}, \tag{A1}$$

where ϵ is, as before, the mean turbulent kinetic energy dissipation rate and N is the Brunt-Väisälä frequency, defined as

$$N = \sqrt{\frac{g}{T}\frac{dT}{dz}}. \tag{A2}$$

In the study used here, no information was provided about the actual mean potential temperature gradient dT/dz. However, an approximated estimate of L_0 for the runs collected in the case of stable atmospheric stratification may be conducted. Note that only four runs follow this stability class as runs not meeting strict stationarity requirements were excluded from the analysis (and they were mainly collected in unstable atmospheric conditions). The mean dT/dz was computed using Monin-Obukhov similarity theory as

$$\frac{dT}{dz} = -\left(\frac{T^*}{K_v z}\right)\phi_T\left(\frac{z}{L}\right), \tag{A3}$$

where $k_v = 0.41$ is the von Kármán constant, $z = 5.1$ m is the distance from the ground, $T^* = \frac{\langle w'T'\rangle}{u^*}$, and for mildly stable stratification

$$\phi_T = \phi_m = 1 + 4.7\left(\frac{z}{L}\right). \tag{A4}$$

The mean turbulent kinetic energy dissipation rate was computed as

$$\epsilon = \frac{u^{*3}}{k_v z}\left(\phi_m - \frac{z}{L}\right). \tag{A5}$$

Figure 11(a) shows that the quantity

$$I_s = \frac{I_w u^* \phi_m}{k_v z} = \text{const} \simeq 0.4 \tag{A6}$$

is almost constant across runs and exhibits a value slightly lower than the expected 0.4.

The estimated values of the dimensionless Ozmidov number $L_0/I_w u^* \phi_m$ are reported in Fig. 11(b). Here L_0 decreases with increasing stability ζ as the effect of buoyancy is experienced

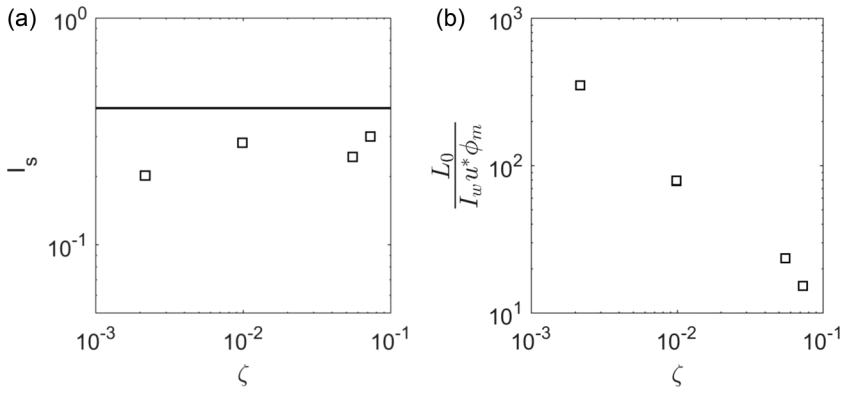

FIG. 11. (a) Quantity I_s and its expected value 0.4 (black horizontal line) for the four stable runs in the data set. (b) Normalized Ozmidov length for the same runs.

by eddies of sizes progressively smaller. However, the values of the Ozmidov scale are consistently larger than the integral scale of the flow I_w for the four stable runs here. Hence, ignoring distortions caused by stable stratification on inertial subrange scales for the aforementioned four runs may be deemed plausible.

[1] K. R. Sreenivasan, Fluid turbulence, Rev. Mod. Phys. **71**, S383 (1999).
[2] B. I. Shraiman and E. D. Siggia, Scalar turbulence, Nature (London) **405**, 639 (2000).
[3] R. A. Antonia, A. J. Chambers, C. A. Friehe, and C. W. Van Atta, Temperature ramps in the atmospheric surface layer, J. Atmos. Sci. **36**, 99 (1979).
[4] Z. Warhaft, Passive scalars in turbulent flows, Annu. Rev. Fluid Mech. **32**, 203 (2000).
[5] J. R. Garratt, Review: The atmospheric boundary layer, Earth Sci. Rev. **37**, 89 (1994).
[6] R. B. Stull, *An Introduction to Boundary Layer Meteorology*, Atmospheric and Oceanographic Science Library Vol. 13 (Springer Science + Business Media, New York, 2012).
[7] A. N. Kolmogorov, The local structure of turbulence in incompressible viscous fluid for very large Reynolds numbers, Dokl. Akad. Nauk SSSR **30**, 301 (1941).
[8] R. H. Kraichnan, Small-scale structure of a scalar field convected by turbulence, Phys. Fluids **11**, 945 (1968).
[9] V. R. Kuznetsov, A. A. Praskovsky, and V. A. Sabelnikov, Fine-scale turbulence structure of intermittent shear flows, J. Fluid Mech. **243**, 595 (1992).
[10] J. Schumacher, J. D. Scheel, D. Krasnov, D. A. Donzis, V. Yakhot, and K. R. Sreenivasan, Small-scale universality in fluid turbulence, Proc. Natl. Acad. Sci. USA **111**, 10961 (2014).
[11] P. K. Yeung, X. M. Zhai, and K. R. Sreenivasan, Extreme events in computational turbulence, Proc. Natl. Acad. Sci. USA **112**, 12633 (2015).
[12] G. G. Katul, C. Manes, A. Porporato, E. Bou-Zeid, and M. Chamecki, Bottlenecks in turbulent kinetic energy spectra predicted from structure function inflections using the von Kármán–Howarth equation, Phys. Rev. E **92**, 033009 (2015).
[13] G. Katul, A. Porporato, D. Cava, and M. Siqueira, An analysis of intermittency, scaling, and surface renewal in atmospheric surface layer turbulence, Physica D **215**, 117 (2006).
[14] A. M. Reynolds, Gusts within plant canopies are extreme value processes, Physica A **391**, 5059 (2012).
[15] H. Xu, A. Pumir, G. Falkovich, E. Bodenschatz, M. Shats, H. Xia, N. Francois, and G. Boffetta, Flight-crash events in turbulence, Proc. Natl. Acad. Sci. USA **111**, 7558 (2014).

[16] G. Falkovich, K. Gawedzki, and M. Vergassola, Particles and fields in fluid turbulence, Rev. Mod. Phys. **73**, 913 (2001).
[17] C. Meneveau, T. S. Lund, and W. H. Cabot, A Lagrangian dynamic subgrid-scale model of turbulence, J. Fluid Mech. **319**, 353 (1996).
[18] F. Porté-Agel, C. Meneveau, and M. B. Parlange, A scale-dependent dynamic model for large-eddy simulation: Application to a neutral atmospheric boundary layer, J. Fluid Mech. **415**, 261 (2000).
[19] C. W. Higgins, M. B. Parlange, and C. Meneveau, Alignment trends of velocity gradients and subgrid-scale fluxes in the turbulent atmospheric boundary layer, Bound.-Layer Meteorol. **109**, 59 (2003).
[20] R. Stoll and F. Porté-Agel, Dynamic subgrid-scale models for momentum and scalar fluxes in large-eddy simulations of neutrally stratified atmospheric boundary layers over heterogeneous terrain, Water Resour. Res. **42** (2006).
[21] G. G. Katul, A. G. Konings, and A. Porporato, Mean Velocity Profile in a Sheared and Thermally Stratified Atmospheric Boundary Layer, Phys. Rev. Lett. **107**, 268502 (2011).
[22] G. G. Katul, D. Li, M. Chamecki, and E. Bou-Zeid, Mean scalar concentration profile in a sheared and thermally stratified atmospheric surface layer, Phys. Rev. E **87**, 023004 (2013).
[23] D. Li, G. G. Katul, and E. Bou-Zeid, Mean velocity and temperature profiles in a sheared diabatic turbulent boundary layer, Phys. Fluids **24**, 105105 (2012).
[24] G. G. Katul, A. Porporato, S. Shah, and E. Bou-Zeid, Two phenomenological constants explain similarity laws in stably stratified turbulence, Phys. Rev. E **89**, 023007 (2014).
[25] D. Li, G. G. Katul, and S. S. Zilitinkevich, Revisiting the turbulent Prandtl number in an idealized atmospheric surface layer, J. Atmos. Sci. **72**, 2394 (2015).
[26] A. S. Monin and A. M. F. Obukhov, Basic laws of turbulent mixing in the surface layer of the atmosphere, Contrib. Geophys. Inst. Acad. Sci. USSR **151**, e187 (1954).
[27] W. Chen, M. D. Novak, T. A. Black, and X. Lee, Coherent eddies and temperature structure functions for three contrasting surfaces. Part I: Ramp model with finite microfront time, Bound.-Layer Meteorol. **84**, 99 (1997).
[28] C. Thomas and T. Foken, Organised motion in a tall spruce canopy: Temporal scales, structure spacing and terrain effects, Bound.-Layer Meteorol. **122**, 123 (2007).
[29] G. Katul, C.-I. Hsieh, and J. Sigmon, Energy-inertial scale interactions for velocity and temperature in the unstable atmospheric surface layer, Bound.-Layer Meteorol. **82**, 49 (1997).
[30] A. M. Obukhov, The local structure of atmospheric turbulence, Dokl. Akad. Nauk. SSSR **67**, 642 (1949).
[31] K. R. Sreenivasan, On local isotropy of passive scalars in turbulent shear flows, Proc. R. Soc. A **434**, 165 (1991).
[32] A. N. Kolmogorov, A refinement of previous hypotheses concerning the local structure of turbulence in a viscous incompressible fluid at high Reynolds number, J. Fluid Mech. **13**, 82 (1962).
[33] G. G. Katul, M. B. Parlange, and C. R. Chu, Intermittency, local isotropy, and non-Gaussian statistics in atmospheric surface layer turbulence, Phys. Fluids **6**, 2480 (1994).
[34] G. Katul, B. Vidakovic, and J. Albertson, Estimating global and local scaling exponents in turbulent flows using discrete wavelet transformations, Phys. Fluids **13**, 241 (2001).
[35] S. B. Pope and E. S. C. Ching, Stationary probability density functions: An exact result, Phys. Fluids A **5**, 1529 (1993).
[36] Y. G. Sinai and V. Yakhot, Limiting Probability Distributions of a Passive Scalar in a Random Velocity Field, Phys. Rev. Lett. **63**, 1962 (1989).
[37] E. S. C. Ching, Probability Densities of Turbulent Temperature Fluctuations, Phys. Rev. Lett. **70**, 283 (1993).
[38] C. W. Gardiner, *Handbook of Stochastic Methods* (Springer, Berlin, 1985), p. 124.
[39] A. Porporato, P. R. Kramer, M. Cassiani, E. Daly, and J. Mattingly, Local kinetic interpretation of entropy production through reversed diffusion, Phys. Rev. E **84**, 041142 (2011).
[40] U. Frisch and D. Sornette, Extreme deviations and applications, J. Phys. (France) I **7**, 1155 (1997).
[41] C. Tsallis, Possible generalization of Boltzmann-Gibbs statistics, J. Stat. Phys. **52**, 479 (1988).
[42] C. Tsallis, S. V. F. Levy, A. M. C. Souza, and R. Maynard, Statistical-Mechanical Foundation of the Ubiquity of Lévy Distributions in Nature, Phys. Rev. Lett. **75**, 3589 (1995).

[43] B. Shi, B. Vidakovic, G. G. Katul, and J. D. Albertson, Assessing the effects of atmospheric stability on the fine structure of surface layer turbulence using local and global multiscale approaches, Phys. Fluids **17**, 055104 (2005).
[44] T. Gotoh and R. H. Kraichnan, Turbulence and Tsallis statistics, Physica D **193**, 231 (2004).
[45] F. M. Ramos, R. R. Rosa, C. R. Neto, M. J. A. Bolzan, L. D. Abreu Sá, and H. F. Campos Velho, Non-extensive statistics and three-dimensional fully developed turbulence, Physica A **295**, 250 (2001).
[46] T. Arimitsu and N. Arimitsu, Tsallis statistics and turbulence, Chaos Soliton. Fractal. **13**, 479 (2002).
[47] M. J. A. Bolzan, F. M. Ramos, L. D. A. Sá, C. Rodrigues Neto, and R. R. Rosa, Analysis of fine-scale canopy turbulence within and above an amazon forest using Tsallis' generalized thermostatistics, J. Geophys. Res.: Atmos. **107** (2002).
[48] L. Mydlarski, A. Pumir, B. I. Shraiman, E. D. Siggia, and Z. Warhaft, Structures and Multipoint Correlators for Turbulent Advection: Predictions and Experiments, Phys. Rev. Lett. **81**, 4373 (1998).
[49] A. J. Lawrance, Directionality and reversibility in time series, Int. Stat. Rev. **59**, 67 (1991).
[50] T. M. Cover and J. A. Thomas, *Elements of Information Theory* (Wiley, New York, 2012), p. 18.
[51] A. Porporato, J. R. Rigby, and E. Daly, Irreversibility and Fluctuation Theorem in Stationary Time Series, Phys. Rev. Lett. **98**, 094101 (2007).
[52] C. Rorai, P. D. Mininni, and A. Pouquet, Stably stratified turbulence in the presence of large-scale forcing, Phys. Rev. E **92**, 013003 (2015).
[53] G. I. Taylor, The spectrum of turbulence, Proc. R. Soc. London Ser. A **164**, 476 (1938).
[54] D. Prichard and J. Theiler, Generating Surrogate Data for Time Series with Several Simultaneously Measured Variables, Phys. Rev. Lett. **73**, 951 (1994).
[55] R. A. Antonia, E. J. Hopfinger, Y. Gagne, and F. Anselmet, Temperature structure functions in turbulent shear flows, Phys. Rev. A **30**, 2704 (1984).
[56] C. Meneveau, K. R. Sreenivasan, P. Kailasnath, and M. S. Fan, Joint multifractal measures: Theory and applications to turbulence, Phys. Rev. A **41**, 894 (1990).
[57] G. Ruiz-Chavarria, C. Baudet, and S. Ciliberto, Scaling laws and dissipation scale of a passive scalar in fully developed turbulence, Physica D **99**, 369 (1996).
[58] R. H. Kraichnan, Anomalous Scaling of a Randomly Advected Passive Scalar, Phys. Rev. Lett. **72**, 1016 (1994).
[59] C. Meneveau, Analysis of turbulence in the orthonormal wavelet representation, J. Fluid Mech. **232**, 469 (1991).
[60] Y. Li and C. Meneveau, Origin of Non-Gaussian Statistics in Hydrodynamic Turbulence, Phys. Rev. Lett. **95**, 164502 (2005).
[61] L. Mydlarski and Z. Warhaft, Passive scalar statistics in high-péclet-number grid turbulence, J. Fluid Mech. **358**, 135 (1998).
[62] J. Lepore and L. Mydlarski, Effect of the Scalar Injection Mechanism on Passive Scalar Structure Functions in a Turbulent Flow, Phys. Rev. Lett. **103**, 034501 (2009).
[63] A. Celani, A. Lanotte, A. Mazzino, and M. Vergassola, Universality and Saturation of Intermittency in Passive Scalar Turbulence, Phys. Rev. Lett. **84**, 2385 (2000).
[64] G. Falkovich, Symmetries of the turbulent state, J. Phys. A: Math. Theor. **42**, 123001 (2009).
[65] R. V. Ozmidov, On the turbulent exchange in a stably stratified ocean, Izv. Acad. Sci. USSR, Atmos. Oceanic Phys. **1**, 861 (1965).
[66] J. P. Dougherty, The anisotropy of turbulence at the meteor level, J. Atmos. Terr. Phys. **21**, 210 (1961).